Aachen Institute for Advanced Study in Computational Engineering Science

Preprint: AICES-2008-9

04/December/2008

Time Integration in the XFEM with Emphasis on Time-stepping

T. P. Fries and A. Zilian

RWTH AACHEN UNIVERSITY

AICES

Financial support from the Deutsche Forschungsgemeinschaft (German Research Association) through grant GSC 111 is gratefully acknowledged.

List of AICES technical reports: http://www.aices.rwth-aachen.de/preprints

Time Integration in the XFEM with Emphasis on Time-stepping

Thomas-Peter Fries, Andreas Zilian

August, 2008

Abstract

The extended finite element method (XFEM) is often used in applications that involve moving interfaces. Examples are the propagation of cracks or the movement of interfaces in two-phase problems. This work focuses on time integration in the XFEM. The performance of the discontinuous Galerkin method in time (space-time finite elements) and time-stepping schemes are analyzed by convergence studies for different model problems. It is shown that space-time finite elements achieve optimal convergence rates. Special care is required for time-stepping in the XFEM due to the time dependence of the enrichment functions. In each time step, the enrichment functions have to be evaluated at different time levels. This has important consequences in the quadrature used for the integration of the weak form. A time-stepping scheme which leads to optimal or only slightly sub-optimal convergence rates is systematically constructed in this work.

Contents

1 Introduction

Moving interfaces are frequently found in the real world and are relevant in many engineering applications. Examples are phase interfaces in solidification problems, the propagation of cracks, and the movement of interfaces between two fluids. The extended finite element method (XFEM) [2, 5] is particularly useful in these applications as it enables the approximation of discontinuities within elements with optimal accuracy. Thereby, fixed meshes can be used throughout the simulations and the moving interfaces are usually captured implicitly by the level-set method [30, 33].

Generally, the XFEM enables a local enrichment of the approximation space. This is realized by means of the partition of unity concept [1, 25]. The enrichment functions employed may enable the approximation to reproduce kinks, jumps, singularities etc. exactly in local parts of the domain. References where the XFEM is used in time depending problems with moving interfaces are e.g. [3, 26] for the simulation of cracks, [11, 21, 27] for solidification problems, and [7, 8, 16, 18] for two-fluid flows. Moving interfaces in the context of fluid-structure interaction with the XFEM are found in [17, 37].

In this work, convergence properties of different time integration methods in the frame of the XFEM for moving interfaces are studied. The authors are not aware of other convergence studies in time for the XFEM. Several instationary model problems are examined: the diffusion equation, the advection-diffusion equation and the Burgers equation. In each model problem, a moving weak discontinuity, i.e. a kink in the sought function, is present. Numerical reference solutions are obtained by means of the standard finite element method (FEM) with high order in space and time. The meshes used for the FEM computations align with the discontinuity, whereas this is not the case for the XFEM simulations using Cartesian meshes. The XFEM simulations are carried out on linear elements with the well-established abs-enrichment in order to capture the weak discontinuity. Problems in partly enriched elements are avoided by using the corrected XFEM of [15]. Similar results are obtained by the modified abs-enrichment of [29]. Herein, we focus on problems with first-order derivatives in time only. Higher-order derivatives in time—such as they appear frequently in solid mechanics—may be converted into first-order problems by standard procedures.

The discontinuous Galerkin method in time is studied first, see e.g. [14, 22] for applications in the standard FEM. This method is used in the XFEM in [9, 10, 31, 37]. Herein, it is found, that the resulting convergence rates in space and time are second order for the

XFEM. This is in contrast to standard linear finite element computations which achieve third-order convergence in time when using the discontinuous Galerkin method in time for the model problems considered in this work [22].

This work focuses on *time-stepping* schemes in the frame of the XFEM as e.g. used in [3, 8, 11, 13, 16, 21]. As noticed already in [9, 10], time-stepping in the XFEM requires special care. The special situation is that the *enrichment* functions in the XFEM are time-dependent (although fixed meshes are used) due to their dependence on the position of the moving discontinuity. When using time-stepping schemes, these functions have to be evaluated at the different time levels involved (typically, t_n and t_{n+1}). As a consequence, there are elements with jumps and/or kinks in the integrands of the weak form resulting from the position of the discontinuity at different time levels. This must considered in the quadrature which, thereby, is considerably more elaborate than for stationary problems.

Different one-step time-stepping schemes are studied and compared: the implicit Euler method, the trapezoidal rule, and the (implicit) midpoint rule. We avoid the frequently used expression "Crank-Nicolson method" for the time integration because there is not always an agreement in the literature whether this refers to the trapezoidal rule [14, 35] or the midpoint rule [28]. It is noted that the trapezoidal and midpoint rule are identical for the diffusion and advection-diffusion equation. However, for the Burgers equation, the results obtained differ significantly. A time-stepping scheme which leads to optimal or only slightly sub-optimal convergence rates is systematically constructed in this work. This method is based on the trapezoidal rule. It is noted that the (implicit) midpoint rule only achieves sub-optimal results and is, therefore, not recommended for use in the XFEM.

This work is organized as follows: Section 2 describes the model problems considered herein. The governing equations are given and the test cases are specified. Section 3 discusses the discontinuous Galerkin method in time. The approximation is based on enriched bi-linear elements in the space-time domain. The numerical results show that second-order convergence is achieved in space and time. Time-stepping schemes are worked out in section 4. In preliminary considerations, it is shown that time should be discretized *before* space which is then realized in section 4.2 and 4.3. The important consequence of time-stepping in the quadrature is discussed in section 4.4. Section 4.5 gives the numerical results and compares different time-stepping schemes. This paper ends in section 5 with a summary and conclusions.

2 Model Problems

Three different instationary model equations are considered for a detailed convergence study: (i) the diffusion equation, (ii) the advection-diffusion equation, and (iii) the Burgers equation (with diffusion). The spatial domain is one-dimensional. For each equation, the diffusion coefficient involves a jump in the domain, the position of the jump is moving with different velocities in space. The resulting approximated functions are weakly discontinuous, i.e. they have a kink where the diffusion coefficient is discontinuous.

We choose these model equations because (i) is a parabolic equation where no numerical problems are expected, i.e. potential problems associated with advection are avoided and stabilization is not an issue [6, 14, 19]. Then, a linear advection term is added for model problem (ii) and we confirm that, in fact, the mathematical properties of the time integration are not influenced. Finally, we choose model problem (iii) because it involves a *non-linear* advection term. In this case, the results for the trapezoidal and midpoint rule for time integration, e.g. [24], are no longer identical. As will be seen, it turns out that the midpoint rule should be avoided in the context of the XFEM.

2.1 Governing equations of model problems

The situation is as follows: A domain $\Omega = (0,1)$ is divided into two time-dependent subdomains $\Omega_1 = (0, x^\star(t))$ and $\Omega_2 = (x^\star(t), 1)$. The boundary is $\Gamma = \partial\Omega$. The initial/boundary value problems for the diffusion equation consists of finding $u(x,t)$ for all $x \in \Omega$ and $t \in (0,T)$ such that

$$u_{,t} = F_{\mathrm{D}} = k_i \cdot u_{,xx} \text{ in } \Omega_i \times (0,T),\ i = 1,2, \tag{2.1}$$

$$u(x,t) = \hat{u}(x,t) \qquad \text{on } \Gamma \times (0,T), \tag{2.2}$$

$$k_1/k_2 \cdot u_{,x}(x^\star - \varepsilon, t) = u_{,x}(x^\star + \varepsilon, t) \text{ for } \varepsilon \to 0, \tag{2.3}$$

$$u(x,0) = u_0(x) \qquad \text{on } \Omega \text{ at } t = 0. \tag{2.4}$$

Equation (2.2) are Dirichlet boundary conditions (no Neumann boundary conditions are present), Equation (2.3) is an interface condition at $x^\star(t)$, and Equation (2.4) is the initial condition. The diffusion coefficients $k_1, k_2 \in \mathbb{R}$, $k_1 \neq k_2$, are discontinuous at $x^\star(t)$. Then, it is obvious from Equation (2.3) that the gradient of $u(x,t)$ is discontinuous there. Thus, u is a weakly discontinuous function in the domain.

For the other two model equations, Equation (2.1) changes to

$$u_{,t} = F_{\mathrm{AD}} = -c \cdot u_{,x} + k_i \cdot u_{,xx} \tag{2.5}$$

for the instationary advection-diffusion equation and

$$u_{,t} = F_{\mathrm{B}} = -u \cdot u_{,x} + k_i \cdot u_{,xx} \tag{2.6}$$

for the Burgers equation, respectively.

The position of the discontinuity at $x^\star$ is time-dependent and given as

$$x^\star(t) = x_A + \frac{x_B - x_A}{T}\, t, \quad x_A, x_B \in \mathbb{R},\ t \in (0, T). \tag{2.7}$$

See Figure 1 for a sketch of the situation. The corresponding constant velocity of the moving discontinuity is

$$v^\star = x^\star_{,t} = \frac{x_B - x_A}{T}. \tag{2.8}$$

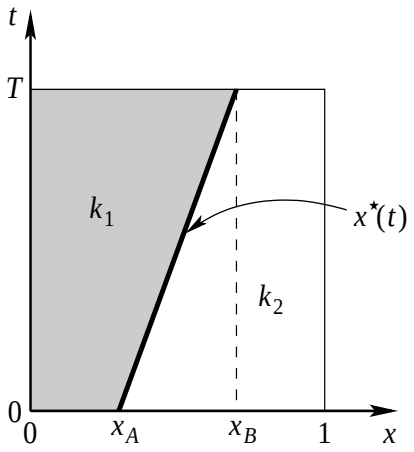

Figure 1: The space-time domain $Q = \Omega \times (0, T)$ with the discontinuity in the diffusion coefficients.

In XFEM applications, the discontinuities are usually within elements, i.e. not aligned with element edges. The position of the discontinuities is often defined by means of the level-set method, see e.g. [30, 33]. Then, the zero-level of a scalar function $\phi(x, t)$ in the domain—called the level-set function—is used for the implicit description of the discontinuity. For the explicit definition of the discontinuity as given in Equation (2.7), a possible level-set

function follows as

$$\phi(x,t) = \frac{(x - x_A)\cdot T + (x_A - x_B)\cdot t}{\sqrt{T^2 + (x_A - x_B)^2}}. \tag{2.9}$$

This level-set function fulfills the signed-distance property. It is zero along the discontinuity, i.e. the line between $(x_A, 0)$ and (x_B, T), and its sign is opposite in Ω_1 and Ω_2.

2.2 Test cases

For the model problems described above in a general way, we now define specific parameters. Our aim is to analyze the performance of time integration schemes with focus on

1. the influence of the velocity of the discontinuity, see Equation (2.8).

2. the influence of the jump in the gradient along the discontinuity, i.e. the ratio of k_1/k_2 as seen in Equation (2.3).

For all test cases shown, analytical solutions to the initial/boundary value problem are not applicable. Therefore, we use numerical reference solutions which are computed by means of a higher-order standard finite element method where the mesh is aligned with the discontinuity, see Figure 2(a). In contrast, all computations with the XFEM are carried out on *bi-linear* finite elements on *Cartesian* meshes as shown in Figure 2(b).

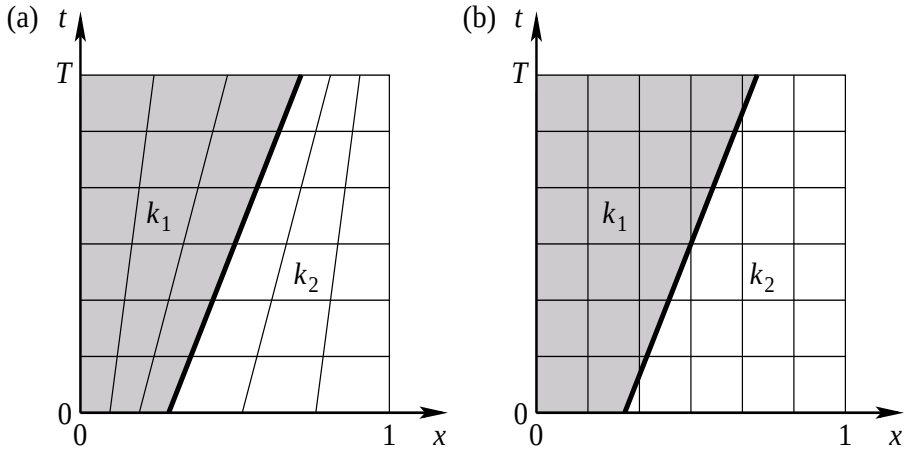

Figure 2: (a) Mesh for standard FEM computations with element edges aligning with the discontinuity, (b) Cartesian mesh used for XFEM computations.

Errors are measured in the L_2-norm at $t = T$ as

$$e = \frac{\sqrt{\int_\Omega \left(u^h(x,T) - u^{\text{ex}}(x,T)\right)^2 d\Omega}}{\sqrt{\int_\Omega \left(u^{\text{ex}}(x,T)\right)^2 d\Omega}} \tag{2.10}$$

where u^h is the approximation and u^{ex} is the numerical reference solution.

2.2.1 Test cases for the diffusion equation

The situation is observed until $T = 1.0$, Dirichlet boundary conditions are set to $u(0,t) = u(1,t) = 0$ for all $t \in (0,T)$. The initial condition is a C_∞-continuous function defined as

$$u_0\left(q\left(x\right)\right) = \begin{cases} \exp\left(5 + \frac{5}{q^2-1}\right) & \text{for } q \leq 1, \\ 0 & \text{else,} \end{cases} \tag{2.11}$$

with $q\left(x\right) = \left|x - x_c\right| / \varrho$. This function is centered at $x_C = 0.5$, and $\varrho = 0.2$ scales the support, see Figure 3(a). We set

$$k_1 = \{2.5,\ 1.0,\ 0.5,\ 0.25,\ 0.1,\ 0.05\} \cdot 10^{-3} \qquad \text{and} \qquad k_2 = 5.0 \cdot 10^{-3}, \tag{2.12}$$

so that different ratios of k_2/k_1 result as $\{2,\ 5,\ 10,\ 20,\ 50,\ 100\}$. The geometric conditions are specified by

$$x_A = \{0.2,\ 0.3,\ 0.4,\ 0.45,\ 0.5\} \quad \text{and} \quad x_B = 1.0 - x_A \tag{2.13}$$

resulting in the velocities $v^\star = \{0.6,\ 0.4,\ 0.2,\ 0.1,\ 0.0\}$ through Equation (2.8). The reference solutions at $t = 1$ for these cases are shown in Figure 3(b) to (f).

The reference solutions are obtained by 100×100 Lagrangean space-time elements with order 8 in space and 7 in time. Using the discontinuous Galerkin method in time [14, 22], which is of order $p + 1$ in time for problems involving first-order time derivatives, this results in an overall convergence rate of order 8. We validate this solution by performing a convergence study with other standard finite elements of order 1, 2, 3, 4, and 5 in space and time for each of the different cases. A typical example of the results is shown in Figure 4 where the L_2-error for different element sizes are shown for the case of $x_A = 0.4$, $x_B = 0.6$, and $k_2/k_1 = 10$. It can be seen that the expected optimal convergence rates are achieved

up to an error level of about 10^{-9}, indicating the high accuracy of the numerical reference solution.

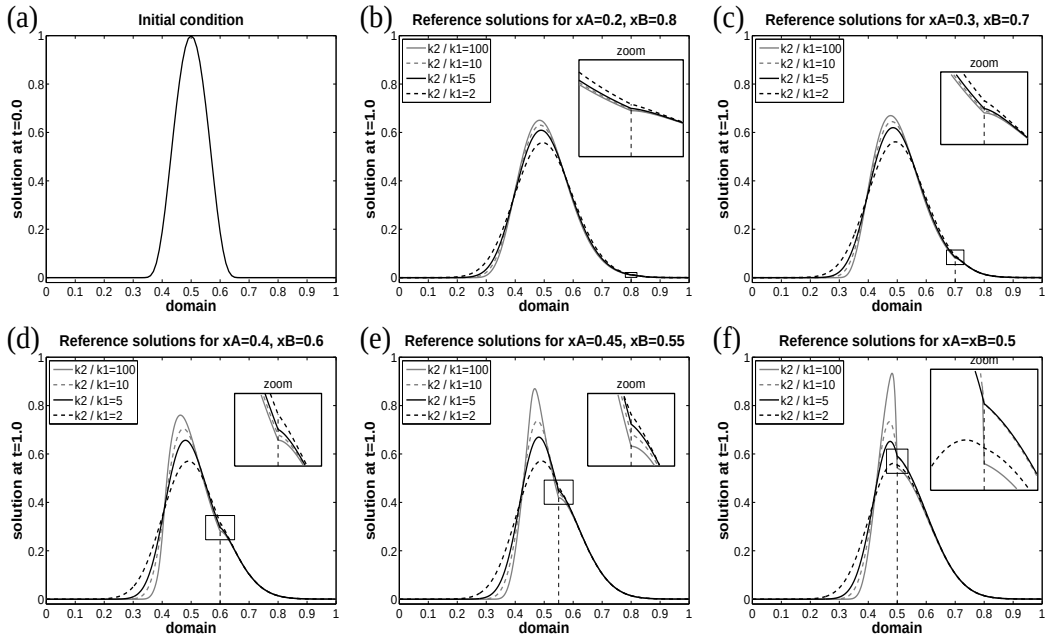

Figure 3: (a) Initial condition for the diffusion test case. Reference solutions at $t = 1$ are shown in (b) to (f) for the different geometric situations and $k_2/k_1 = \{2,\ 5,\ 10,\ 100\}$. The zoom boxes illustrate the kink at $x^\star(T) = x_B$.

2.2.2 Test cases for the advection-diffusion equation

Most parameters are chosen as for the pure diffusion case described in section 2.2.1. The initial condition is defined as in Equation (2.11), however, the exponential function is now centered at $x_C = 0.25$ with a support scaled by $\varrho = 0.2$, see Figure 5(a). The advection velocity c in Equation (2.5) is set to $c = 0.3$. The different values for k_1 and k_2 in Equation (2.12) are restricted to the ones where $k_2/k_1 = \{2,\ 5,\ 10\}$ because for higher ratios, oscillations appeared in the numerical reference solutions as well as for the XFEM results. This is due to the advection of locally steep gradients for high k_2/k_1-ratios.

Reference solutions for the different geometric cases (x_A and x_B) and ratios of the diffusion coefficients (k_2/k_1) at $t = 1$ are shown in Figure 5(b) to (f). These reference solutions have been validated as described above.

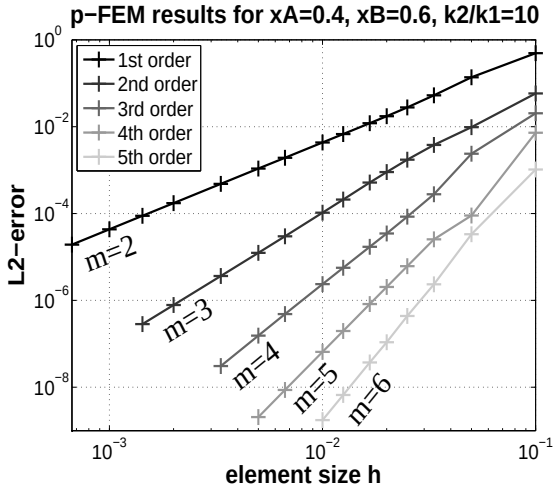

Figure 4: Convergence study for the p-version of the standard FEM for the diffusion equation. The convergence rate is denoted by m.

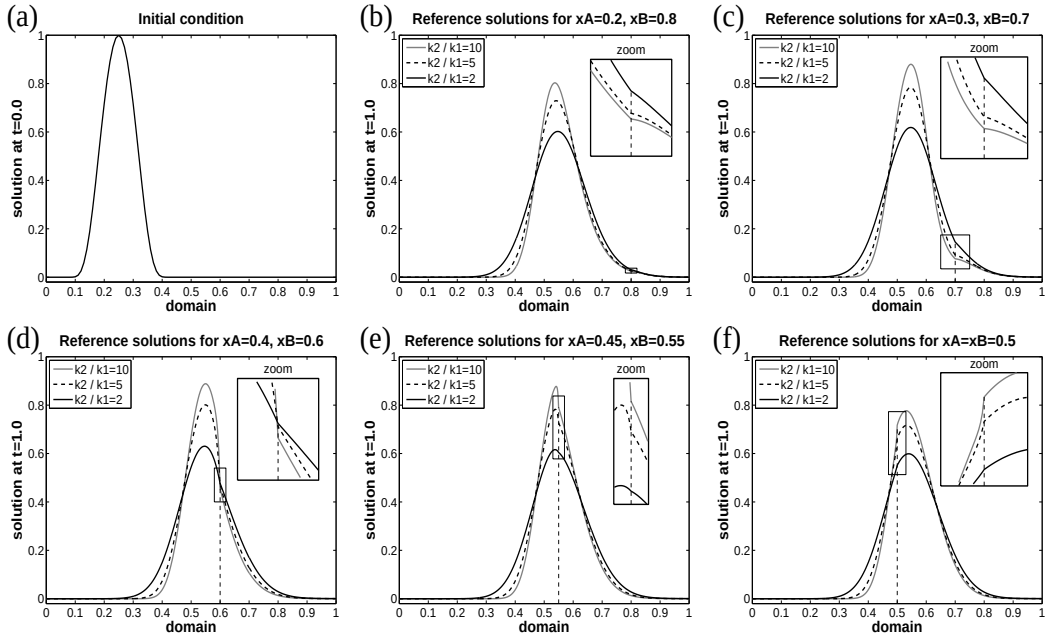

Figure 5: (a) Initial condition for the advection-diffusion test case. Reference solutions at $t = 1$ are shown in (b) to (f) for the different geometric situations. The zoom boxes illustrate the kink at $x^\star(T) = x_B$.

2.2.3 Test cases for the Burgers equation

The time interval is now reduced to $T = 0.2$ (because for $T = 1$ the solution is rather close to zero for some k_1/k_2). For all computations (FEM and XFEM), the ratio of the spatial domain $\Omega = (0, 1)$ to the temporal domain $(0, T)$ of $5 : 1$ is also reflected in the element numbers. That is, five times more elements are used in space than in time. The initial condition is

$$u_0(x) = \sin(\pi \cdot x) \tag{2.14}$$

and is shown in Figure 6(a).

The diffusion coefficients are set to

$$k_1 = 1.0 \qquad \text{and} \qquad k_2 = \{0.5,\ 0.2,\ 0.1,\ 0.01\}, \tag{2.15}$$

so that different ratios of k_1/k_2 result as $\{2,\ 5,\ 10,\ 100\}$. The geometric conditions are specified by

$$x_A = \{0.2,\ 0.3,\ 0.4,\ 0.44,\ 0.46,\ 0.48,\ 0.49,\ 0.5\} \quad \text{and} \quad x_B = 1.0 - x_A \tag{2.16}$$

resulting in the discontinuity velocities of

$$v^\star = \{3.0,\ 2.0,\ 1.0,\ 0.6,\ 0.4,\ 0.2,\ 0.1,\ 0.0\} \tag{2.17}$$

through Equation (2.8). The reference solutions at $t = 0.2$ for these cases are shown in Figure 6(b) to (f) for $x_A = \{0.2,\ 0.3,\ 0.4,\ 0.46,\ 0.5\}$, respectively.

3 Space-time finite elements

In this section, the model equations given in the previous section are discretized using the discontinuous Galerkin method in time, see e.g. [14, 22] and references given therein. For applications of this method in the context of the XFEM, see [9, 10, 37]. The space-time domain $\Omega \times (0, T)$ is divided into time slabs $Q_n = \Omega \times (t_n, t_{n+1})$, where $0 = t_0 < t_1 < \ldots < t_{\mathrm{N}} = T$. Each time slab is discretized by extended space-time finite elements. The

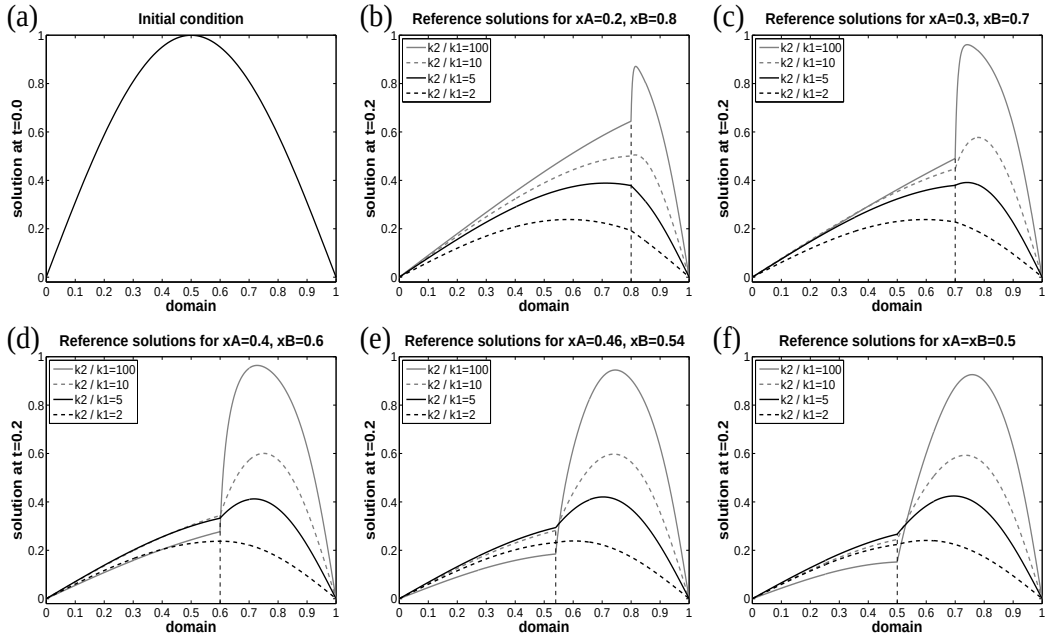

Figure 6: (a) Initial condition for the Burgers test case. Reference solutions at $t = 0.2$ are shown in (b) to (f) for the different geometric situations.

enriched approximation is of the form

$$u^h(x,t) = \underbrace{\sum_{i\in I} N_i(x,t)\, u_i}_{\text{strd. FE approx.}} + \underbrace{\sum_{i\in I^\star} M_i(x,t)\, a_i}_{\text{enrichment}}, \tag{3.1}$$

where $N_i(x,t)$ are bi-linear finite element functions. I is the set of all nodes in the domain, and $I^\star$ is the set of enriched nodes, $I^\star \subset I$. $M_i(x,t)$ are called local enrichment functions and useful definitions of these functions enable optimal accuracy for weakly discontinuous fields without any alignment of the kinks with element edges.

One way to define these functions is

$$M_i(x,t) = N_i(x,t) \cdot [\psi(x,t) - \psi(x_i,t_i)] \quad \forall i \in I^\star, \tag{3.2}$$

where $\psi(x,t)$ is called enrichment function. For weak discontinuities, the abs-enrichment is well-established, then,

$$\psi(x,t) = \mathrm{abs}(\phi(x,t)), \tag{3.3}$$

where $\phi(x,t)$ is the level-set function of Equation (2.9). $I^\star$ is the set of nodes of all elements

cut by the discontinuity. This definition, though straightforward, is known to introduce problems in partly enriched elements (only some of the element nodes are enriched, i.e. in $I^\star$) resulting in sub-optimal convergence rates. The problems resulting in these so-called blending elements are discussed in detail in [12, 15]. There are many ways to improve the situation for weak discontinuities, e.g.

- The use of enhanced strain techniques in blending elements with the aim to cancel out problematic terms [12].
- The choice of appropriate combinations of the finite element (FE) shape functions in the standard and enriched part of the approximation [12]. For example, choosing FE functions of order $p+1$ in the standard part and of order p in the enriched part, see Equation (3.2).
- Smoothing techniques in the blending elements, as e.g. used in [34].
- Using a modified abs-enrichment function [29], which is zero in the blending elements, rather than the one given in Equation (3.3).
- Using the "corrected XFEM" as proposed in [15].

Here, we use the corrected XFEM which has been shown to achieve optimal convergence for weak discontinuities in [15]. The local enrichment functions are then defined as

$$M_i\left(x,t\right) = N_i\left(x,t\right) \cdot \left[\psi\left(x,t\right) - \psi\left(x_i,t_i\right)\right] \cdot R(x,t) \quad \forall i \in I^\star, \tag{3.4}$$

where $R(x,t)$ is a ramp function

$$R(x,t) = \sum_{i \in I'} N_i(x,t). \tag{3.5}$$

I' is the set of nodes of all elements cut by the discontinuity. $I^\star$ includes I' plus all nodes of elements next to the cut elements, see Figure 7. We have also realized and analyzed the modified abs-enrichment of [29]; no significant differences to the results obtained by the corrected XFEM have been found.

The following test and trial function spaces $\mathcal{S}_n^h$ and $\mathcal{V}_n^h$ are introduced as

$$\mathcal{S}_n^h = \left\{ u^h \middle| \, u^h \in \mathcal{H}^{1h},\, u^h = \hat{u}^h \text{ on } \Gamma \times (t_n, t_{n+1}) \right\}, \tag{3.6}$$

$$\mathcal{V}_n^h = \left\{ w^h \middle| \, w^h \in \mathcal{H}^{1h},\, w^h = 0 \text{ on } \Gamma \times (t_n, t_{n+1}) \right\}, \tag{3.7}$$

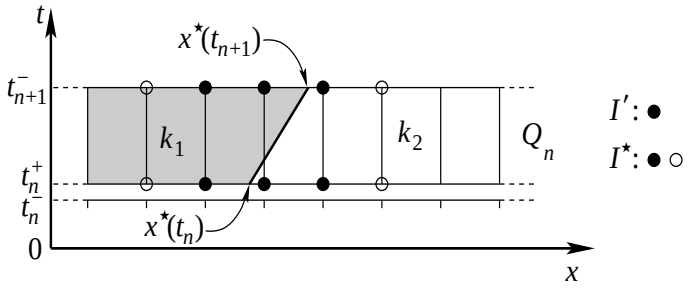

Figure 7: Nodal sets $I^\star$ and I' in the time slab Q_n.

where $\mathcal{H}^{1h} \subseteq \mathcal{H}^1$ is a finite dimensional Hilbert space consisting of the shape functions defined above. The space $\mathcal{H}^1$ is the set of functions which are, together with their first derivatives, square-integrable in Ω. The discretized weak forms for the three model problems may be formulated in the following Bubnov-Galerkin setting [4, 36]: Given $\left(u^h\right)_n^-$, find $u^h \in \mathcal{S}_n^h$ such that $\forall w^h \in \mathcal{V}_n^h$

$$\int_{Q_n} w^h \cdot f^h(x,t) \cdot u^h_{,x}\, dQ + k_i \int_{Q_n} w^h_{,x} \cdot u^h_{,x}\, dQ \tag{3.8}$$

$$+ \int_{\Omega_n} \left(w^h\right)_n^+ \cdot \left(\left(u^h\right)_n^+ - \left(u^h\right)_n^-\right) d\Omega \;=\; 0, \tag{3.9}$$

where

$$f^h(x,t) \;=\; \begin{cases} 0 & \text{for the diffusion equation,} \\ c \in \mathbb{R} & \text{for the advection-diffusion equation,} \\ u^h(x,t) & \text{for the Burgers equation.} \end{cases} \tag{3.10}$$

The notation $\left(u^h\right)_n^\pm$ is

$$\left(u^h\right)_n^\pm = \lim_{\varepsilon \to 0} u^h\left(x, t_n \pm \varepsilon\right). \tag{3.11}$$

It may be seen on the left hand side of Equation (3.9) that the continuity of u^h is enforced weakly across the space-time slab boundaries.

3.1 Numerical results

The convergence properties are now studied for the XFEM employing the discontinuous Galerkin method in time. For the convergence studies, the following numbers of elements

are used in space (n_x) and time (n_y)

$$N = \{10, 20, 30, 40, 50, 60, 80, 100, 150, 200, 300, 500, 700, 1000, 1500, 2000, 2500, 3000, 4000, 5000, 7000, 10000\} \tag{3.12}$$

$$n_x = N - 1 \tag{3.13}$$

$$n_y = \begin{cases} N/5 & \text{for the Burgers equation} \\ N & \text{otherwise.} \end{cases} \tag{3.14}$$

Results for the three model equations are shown in Figure 8(a) to (c), respectively. Only the results with the highest ratios for k_1/k_2 (or k_2/k_1) are shown for each test case. Different geometric situation are considered, characterized by x_A and x_B. Note that the larger the difference between x_A and x_B is, the higher is the velocity of the discontinuity, see Equation (2.8). It may be seen in Figure 8(c) that, often, higher velocities lead to larger errors. However, for all model problems, the convergence rates achieved are *always* of order 2, irrespective of the ratio k_1/k_2 and the velocity of the discontinuity.

In Figure 9, the temporal errors of the FEM and XFEM are studied in the context of space-time elements for the diffusion equation. For this study, $x_A = 0.2$, $x_B = 0.8$ and $k_2/k_1 = 2$. The spatial resolution $h = 1/n_x$ is very small compared to the temporal resolution $\Delta t = 1/n_y$. As a consequence, the resulting spatial error is negligible and the approximation error is dominated by the temporal error. As can be seen in Figure 9(a), the standard FEM (on meshes which align with the discontinuity) is third-order accurate in time, whereas the XFEM (on Cartesian meshes) is second order. We conclude that the extra order in time which is gained for the standard FEM using the discontinuous Galerkin method in time is lost in the XFEM. On the other hand, a second-order convergence in time is still a very good result as the overall approximation error is "only" second order anyway (due to the spatial error).

4 Time-stepping in the XFEM

Finite differences in the context of the XFEM have been used e.g. in [3, 8, 11, 13, 16, 21]. It is mentioned in [9, 10], that space time elements as discussed in section 3 are a natural choice in the frame of the XFEM and that time-stepping requires special care. Here, we systematically construct a time-stepping scheme which leads to optimal or only slightly sub-optimal convergence rates.

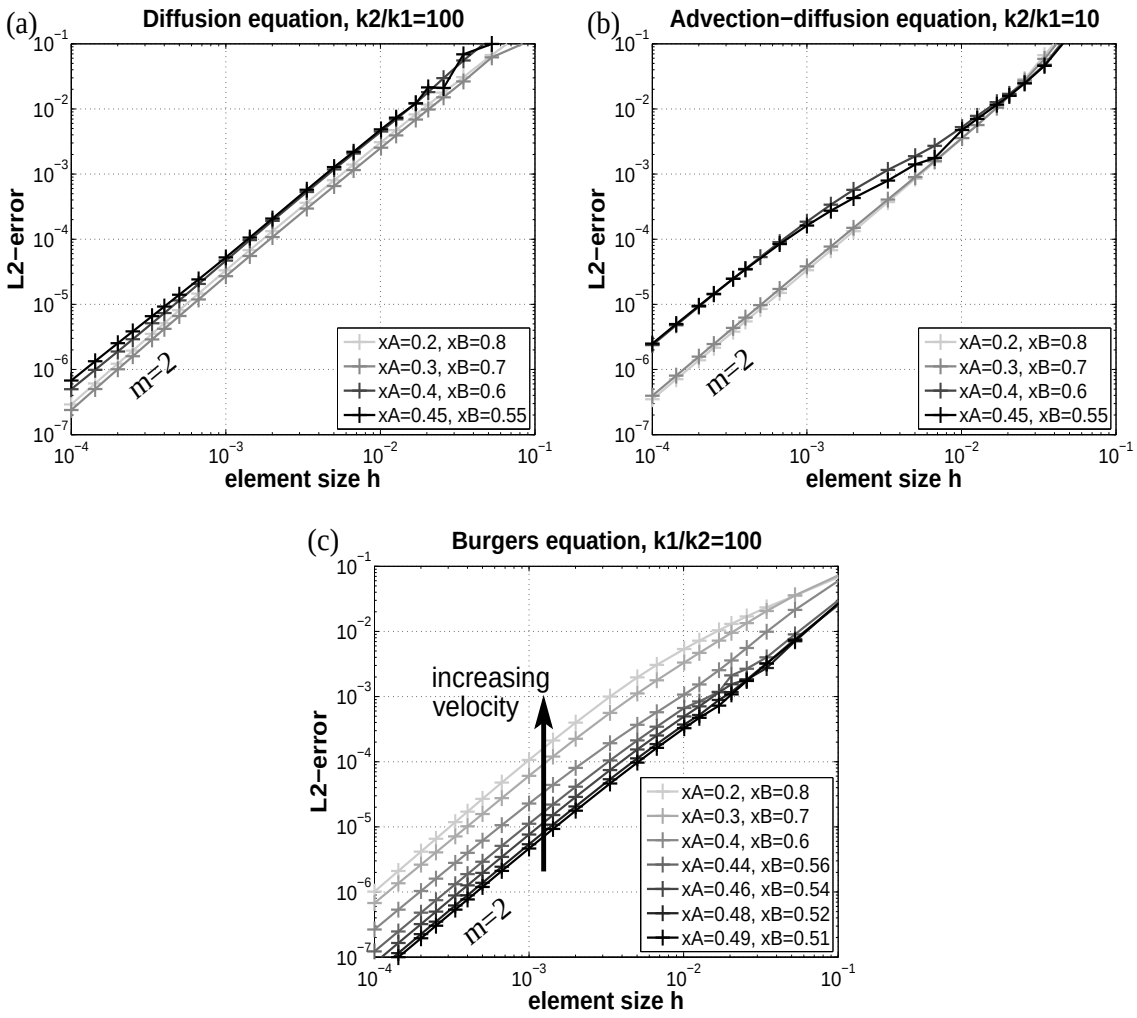

Figure 8: Convergence results for the XFEM employing the discontinuous Galerkin method in time. (a) shows the results for the diffusion equation, (b) for the advection-diffusion equation, and (c) for the Burgers equation. The convergence rate is denoted by m.

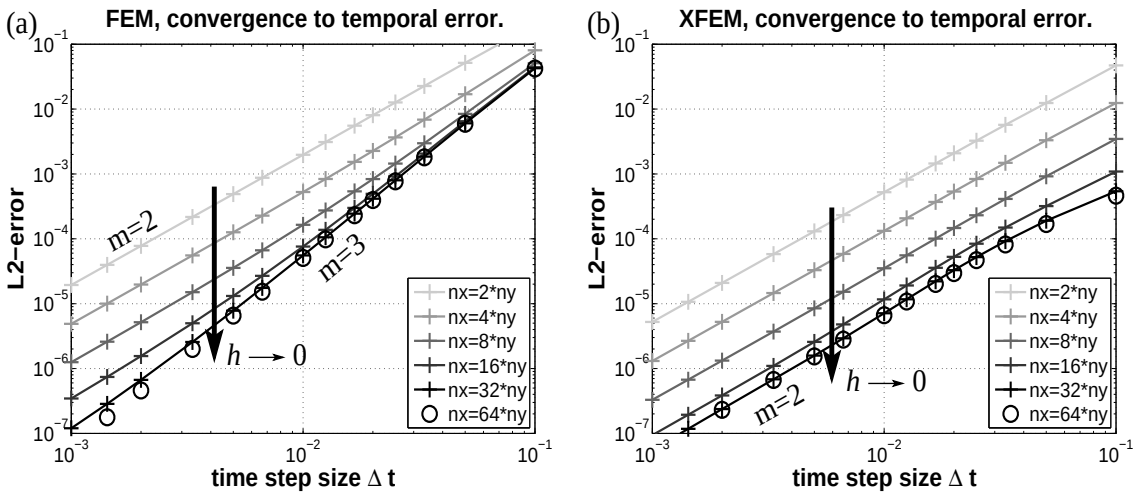

Figure 9: Convergence to the temporal error for the discontinuous Galerkin method in time for the (a) FEM and (b) XFEM, m denotes the convergence rate.

Different one-step time-stepping schemes are studied and compared. In what follows, time is discretized by n_y time steps. The time step size is constant as $\Delta t = n_y/T$. In each time step, t_n refers to the time level where the solution is known from the previous time step and t_{n+1} is the time level where the solution of the current time step is to be computed.

Let us first point out the important difference between time-stepping in the standard FEM and in the XFEM for moving discontinuities. Standard finite element functions rely directly on the mesh used during the simulation. For fixed meshes throughout the computation, the standard FE shape functions are constant in time. Moving meshes are usually treated by Arbitrary-Lagrangian-Eulerian (ALE) formulations of the underlying equations, e.g. [14, 20]. Then, the time dependence is shifted to a so-called mesh velocity and all FE shape functions are evaluated at time level t_{n+1}. A cumbersome evaluation of shape functions on meshes at different time levels is thereby avoided.

In XFEM computations, the shape functions consist in standard finite element functions N_i and enrichment functions M_i. Typically, the meshes remain fixed in XFEM applications which also holds for all examples shown here. As a consequence, the standard finite element functions remain constant in time. However, *this is not the case for the enrichment functions* in the presence of moving discontinuities. The movement of the discontinuity is reflected in a time-dependent level-set function $\phi(x,t)$. The enrichment functions are based on this level-set function, i.e. $M_i(\phi)$, and are, thus, inherently time-dependent as well.

This is summarized as follows: Standard FEM simulations on fixed meshes involve shape functions that are constant in time. In contrast, XFEM simulations on fixed meshes in the presence of moving discontinuities involve some shape functions (the enrichment functions) which are time-dependent . The consequences for time-stepping in the XFEM are analyzed within this work.

Remark 1 XFEM applications on moving meshes may also be considered in an ALE framework, see e.g. [23]. However, this does only solve the problem of different shape functions at time level t_n and t_{n+1} for the standard FE shape functions. The issue of time-dependent enrichment functions remains.

Remark 2 The fact that for the standard FEM on moving meshes, the problem of different shape functions at time level t_n and t_{n+1} can be solved through the ALE framework, i.e. by use of a mesh velocity which is subtracted from the physical *advection velocity*, brings up an interesting question: Is it possible to solve the problem of different enrichment functions at t_n and t_{n+1} in the XFEM on fixed meshes by considering a *discontinuity velocity*? This question will not be answered within this work, but left as an open question which deserves further investigation.

4.1 Preliminary considerations

When using time-stepping schemes, a decision has to be made which of the two discretizations—spatial or temporal—has to be carried out first. When time-dependent problems (involving first-order derivatives in time) are first discretized with respect to the spatial variables, this leads to a system of coupled first-order differential equations in time. This procedure is called semi-discrete method, see e.g. [14]. For the approximation of the system of ordinary differential equations, a variety of sophisticated numerical methods apply. This technique is often known under the name method of lines, see e.g. [14, 32, 35]. However, for this approach, it is required that the shape functions do not depend on time and the time dependence is accounted for by the nodal values. That is, the approximation can be written in the form

$$u^h(x,t) = \sum_i \mathcal{N}_i(x)\,\mathcal{U}_i(t) \tag{4.1}$$

where $\mathcal{N}_i$ and $\mathcal{U}_i$ are now, respectively, all shape functions and coefficients used (i.e. of the standard FE *and* the enriched part). This, however, is not possible for the case of the XFEM including moving discontinuities, because of the inherent time dependence of the enrichment functions. Thus, we conclude that time should be discretized *before* space.

4.2 Temporal discretization

All three model problems given in Equations (2.1), (2.5), and (2.6) may be written in the form

$$u_{,t} = F(u,t) \tag{4.2}$$

$$= \begin{cases} F_{\mathrm{D}}, \text{ for the diffusion equation,} \\ F_{\mathrm{AD}}, \text{ for the advection-diffusion equation,} \\ F_{\mathrm{B}}, \text{ for the Burgers equation.} \end{cases} \tag{4.3}$$

The following time-stepping schemes are analyzed: implicit Euler, trapezoidal rule, and (implicit) midpoint rule. When using an implicit Euler scheme in time, the partial differential equation (4.2) is replaced by

$$\frac{u_{n+1} - u_n}{\Delta t} = F\left(u_{n+1}, t_{n+1}\right), \tag{4.4}$$

where Δt is the time step size. For the trapezoidal rule we use

$$\frac{u_{n+1} - u_n}{\Delta t} = \theta \cdot F\left(u_{n+1}, t_{n+1}\right) + (1-\theta) \cdot F\left(u_n, t_n\right), \quad \theta = \frac{1}{2}, \tag{4.5}$$

and for the midpoint rule

$$\frac{u_{n+1} - u_n}{\Delta t} = F\left(\left(\theta \cdot u_{n+1} + (1-\theta) \cdot u_n\right), \left(\theta \cdot t_{n+1} + (1-\theta) \cdot t_n\right)\right), \quad \theta = \frac{1}{2}, \tag{4.6}$$

$$= F\left(u_\theta, t_\theta\right). \tag{4.7}$$

For linear, autonomous problems as is the case for the diffusion and advection-diffusion equations, (2.1) and (2.5), the trapezoidal and midpoint rule coincide. The notation is $u_{n+1} = u(x, t_{n+1})$ and $u_n = u(x, t_n)$.

4.3 Spatial discretization

Let us now define approximations for $u(x,t)$ used in the time-discretized expressions given above. In contrast to extended space-time elements, the enriched approximation is now defined at particular time levels t_k as

$$u_k^h = u^h(x,t_k) = \underbrace{\sum_{i\in I_k} N_i(x)\, u_i}_{\text{strd. FE approx.}} + \underbrace{\sum_{i\in I_k^\star} M_i(x,t_k)\, a_i}_{\text{enrichment}}. \tag{4.8}$$

It may be seen that this is a *one*-dimensional approximation, which is in contrast to the two-dimensional space-time approximation in Equation (3.1). $N_i(x)$ are one-dimensional linear finite element functions and $M_i(x,t_k)$ are one-dimensional local enrichment functions defined as

$$M_i(x,t_k) = N_i(x)\cdot[\psi(x,t_k) - \psi(x_i,t_k)]\cdot R(x,t_k) \quad \forall i \in I_k^\star, \tag{4.9}$$

where $\psi(x,t)$ is the enrichment function of Equation (3.3). The same remarks about blending elements from section 3 apply for the one-dimensional situation, wherefore also the corrected XFEM is employed now [15]. This is reflected by the choice of the nodal set $I_k^\star$ as the set of element nodes of all cut elements at time level t_k *and* their neighboring elements, see Figure 10. Furthermore, a ramp function is involved which is defined as

$$R(x,t_k) = \sum_{i\in I_k'} N_i(x) \tag{4.10}$$

where I_k' is the set of element nodes of all cut elements at time level t_k, see Figure 10.

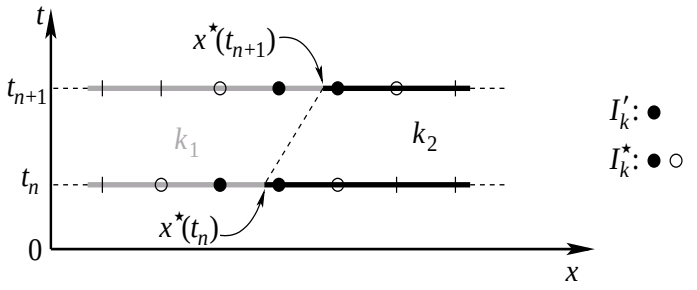

Figure 10: Nodal sets $I_k^\star$ and I_k' at time levels t_k with $k = \{n, n+1\}$.

The discretized weak forms for the three different time-stepping schemes (4.4) to (4.6) result as follows: Given u_0^h, find $u^h \in \mathcal{S}^h$ such that $\forall w^h \in \mathcal{V}^h$

(implicit Euler)

$$\begin{aligned} &\tfrac{1}{\Delta t}\int_\Omega w^h \cdot u^h_{n+1}\,d\Omega + \int_\Omega w^h \cdot f^h_{n+1}\cdot \left(u^h_{n+1}\right)_{,x}\,d\Omega + \int_\Omega k_{n+1} w^h_{,x}\cdot \left(u^h_{n+1}\right)_{,x}\,d\Omega \\ &\qquad = \tfrac{1}{\Delta t}\int_\Omega w^h \cdot u^h_n\,d\Omega \end{aligned} \tag{4.11}$$

(trapezoidal rule)

$$\begin{aligned} &\tfrac{1}{\Delta t}\int_\Omega w^h \cdot u^h_{n+1}\,d\Omega + \theta\int_\Omega w^h \cdot f^h_{n+1}\cdot \left(u^h_{n+1}\right)_{,x}\,d\Omega + \theta\int_\Omega k_{n+1} w^h_{,x}\cdot \left(u^h_{n+1}\right)_{,x}\,d\Omega \\ &= \tfrac{1}{\Delta t}\int_\Omega w^h \cdot u^h_n\,d\Omega - (1-\theta)\int_\Omega w^h \cdot f^h_n\cdot \left(u^h_n\right)_{,x}\,d\Omega - (1-\theta)\int_\Omega k_n w^h_{,x}\cdot \left(u^h_n\right)_{,x}\,d\Omega \end{aligned} \tag{4.12}$$

(midpoint rule)

$$\begin{aligned} &\tfrac{1}{\Delta t}\int_\Omega w^h \cdot u^h_{n+1}\,d\Omega + \int_\Omega w^h \cdot f^h_\theta\cdot \left(u^h_\theta\right)_{,x}\,d\Omega + \int_\Omega k_\theta w^h_{,x}\cdot \left(u^h_\theta\right)_{,x}\,d\Omega \\ &\qquad = \tfrac{1}{\Delta t}\int_\Omega w^h \cdot u^h_n\,d\Omega \end{aligned} \tag{4.13}$$

Here, we think of the diffusion parameter as a function

$$k_m = k(x,t_m) = \begin{cases} k_1 & \text{for } x \le x^\star(t_m)\,, \\ k_2 & \text{for } x > x^\star(t_m)\,. \end{cases} \tag{4.14}$$

Then, it can be shown that the interface condition (2.3) is automatically fulfilled by the weak forms. Again, f^h_m is used in order to distinguish between the three model problems as

$$f^h_m \;=\; \begin{cases} 0 & \text{for the diffusion equation,} \\ c\in\mathbb{R} & \text{for the advection-diffusion equation,} \\ u^h_m & \text{for the Burgers equation.} \end{cases} \tag{4.15}$$

The test and trial spaces have not yet been defined for this case. The trial space consists in the functions $\{N_i, M_i\}$ of Equation (4.8) at time level $k = n+1$ (we are not concerned with boundary restrictions for simplicity). The same space is used for the test functions. In [9], it is mentioned that the time level which is chosen for the test functions is ambiguous ("ambiguity in the choice of the test function"). However, it turns out that it is, in fact, crucial to choose the same time level for the test *and* trial functions. Otherwise, the regularity of the system matrix can not be guaranteed. This is due to the fact that in the XFEM, in each time level, a different set of enriched nodes and, consequently, of enrichment functions is used in general. When using test and trial functions at different time levels,

it may thus be possible that, at a certain node, a trial function exists whereas no test function is defined there. Consequently, in the weak forms (4.11) to (4.13)

$$w^h = w^h_{n+1} \qquad \text{and} \qquad w^h_{,x} = \left(w^h_{n+1}\right)_{,x}. \tag{4.16}$$

4.4 Integrals with functions at different time levels

It is noted that some integrals in the weak forms (4.11) to (4.13) involve functions evaluated at time level t_n and t_{n+1}, e.g.

$$\frac{1}{\Delta t}\int_\Omega w^h_{n+1} \cdot u^h_n \, d\Omega. \tag{4.17}$$

Therefore, in each time step, level-set functions $\phi_n = \phi(x, t_n)$ and $\phi_{n+1} = \phi(x, t_{n+1})$ are required in order to compute the enrichment functions $M_i(x, t_n)$ and $M_i(x, t_{n+1})$, respectively. An important consequence is that jumps and kinks in $M_i(x, t_n)$ and $M_i(x, t_{n+1})$ occur at different places in the spatial domain. This must be considered in the quadrature of the weak form.

In the XFEM, the integration points are located such that the jumps and/or kinks in the integrand are accounted for appropriately. This is usually achieved by sub-dividing the element areas into polygons for integration purposes. For stationary situations, there is usually one discontinuity inside the domain. However, for the current instationary situations, where enrichment functions with respect to t_n and t_{n+1} are present in the integrals, it is possible that two discontinuities are present within one element, see Fig. 11(a) and (b). This needs to be considered in the quadrature as shown in Fig. 11(c). The numerical integration is thereby considerably more elaborate than for stationary model equations.

We show by a numerical example that it is important to (i) evaluate enrichment functions at different time levels, and (ii) use an appropriate quadrature which considers the location of the *two* discontinuities defined by ϕ_n and ϕ_{n+1}. First, the diffusion equation is considered which is discretized in time by the implicit Euler scheme, see Equation (4.11). We set $x_A = 0.4$, $x_B = 0.6$ and $k_2/k_1 = 10$. In order to specify the different numbers of elements used in the convergence studies we introduce

$$N = \{10, 20, 30, 40, 50, 60, 80, 100, 150, 200, 300, 500, 700, 1000, 1500\}. \tag{4.18}$$

For this study, the numbers of elements in space are $n_x = N - 1$. Two situations are com-

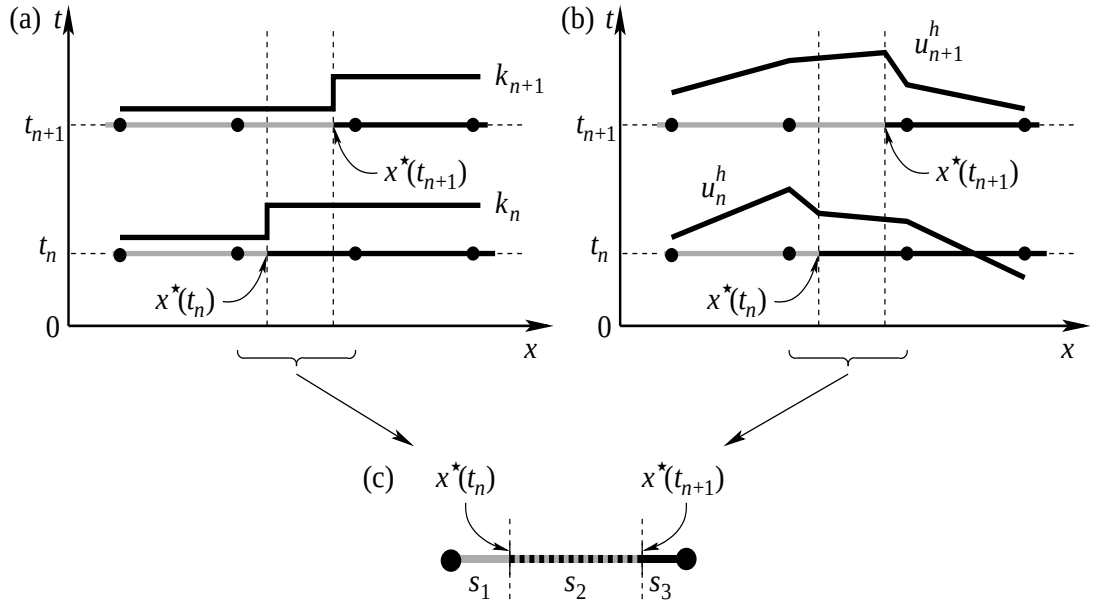

Figure 11: When using time-stepping in the XFEM there are two discontinuities defined by ϕ_n and ϕ_{n+1}. As a consequence, (a) k_n/k_{n+1} and (b) u^h_n/u^h_{n+1} may have a jump/kink at different places within *one* element. (c) shows the decomposition of the cut element into *three* segments s_i for integration purposes.

pared: Alternative 1 evaluates the enrichment functions correctly at t_n and t_{n+1} together with an appropriate integration scheme. Alternative 2 uses enrichment functions based *only* on ϕ_{n+1}. That is, although the coefficients u_i and a_i, see Equation (4.8), are taken correctly from the previous time step, u^h_n is not interpolated correctly.

Figure 12(a) and (b) show the results for the spatial error. The spatial error is achieved by $\Delta t \to 0$. Here, taking $n_y = 64 \cdot N$ elements in time direction was sufficient to extract the spatial error, which is clearly seen in the figures. Most importantly, the *spatial* error is only first order for alternative 2 but second order for alternative 1. It is noted that the temporal error is first order due to the implicit Euler scheme used. This can be seen by the decrease in the convergence rate in Figure 12(a) once the temporal error dominates the spatial error. One can clearly see that second-order convergence in space is only possible when shape functions at time level t_n and t_{n+1} are used.

Next, we analyze the influence of the quadrature. Therefore, we introduce alternative 3 which evaluates the shape functions correctly at t_n and t_{n+1}, but uses a decomposition of the elements into polygons for integration purposes only based on the discontinuity defined by ϕ_{n+1}. Results are shown in Figure 13 for the spatial error. Obviously, the simplified integration scheme of variant 3 reduces the convergence rate, whereas the "correct" quadra-

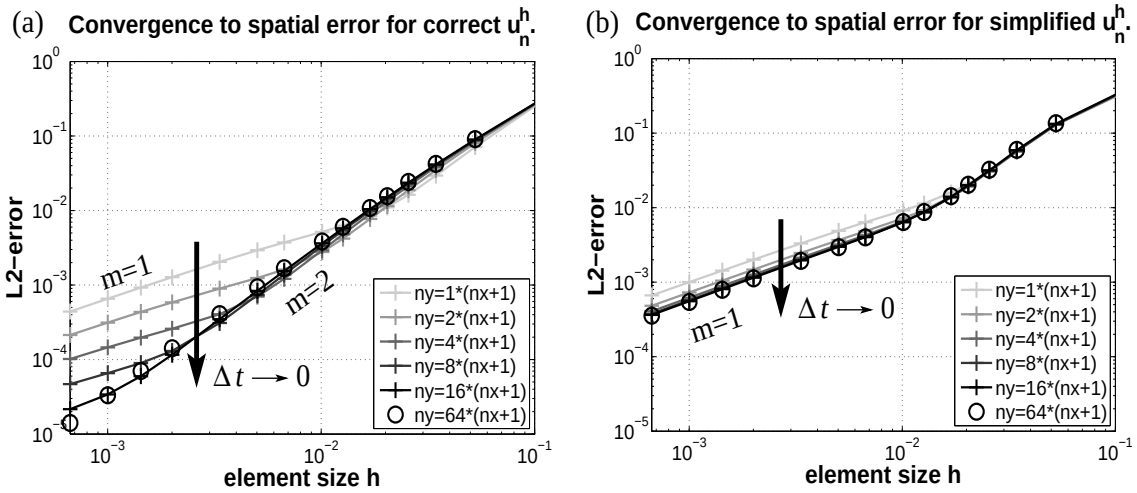

Figure 12: Convergence results for the correct and simplified interpolation of u_n^h, m denotes the convergence rate.

ture achieves optimal results. It is noted, that for alternative 1, the results for $n_y = q \cdot N$ with $q = \{16, 32, 64\}$ are almost identical (i.e. the difference is within the line-width) whereas this is not the case for alternative 3.

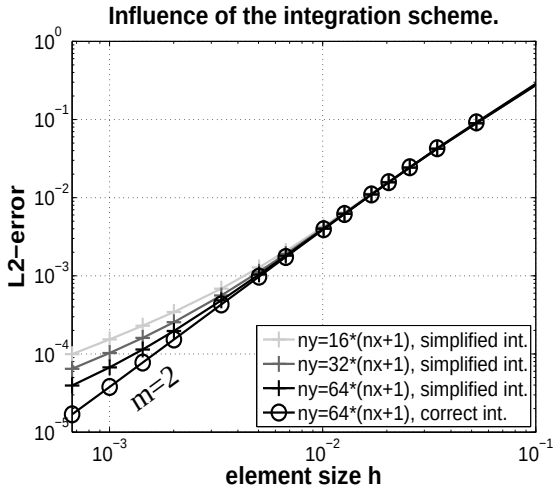

Figure 13: Comparison of a "correct" integration scheme which considers the discontinuities described by ϕ_n and ϕ_{n+1} and a simplified version which only considers the discontinuity at t_{n+1}.

In what follows, based on these findings, all time-stepping schemes evaluate enrichment functions at different time levels, and use an appropriate quadrature which considers the location of the *two* discontinuities defined by ϕ_n and ϕ_{n+1}. Then, the spatial error is optimal, i.e. of order 2.

4.5 Numerical results

The following results are computed by the trapezoidal rule unless noted otherwise. The number of elements in space is $n_x = N-1$, with N given in Equation (4.18), in some cases even more elements are used. In time, the number of elements is $n_y = N$ for the diffusion and advection-diffusion equation and $n_y = N/5$ for the Burgers equation. Thereby, choosing an odd element number in space and even in time, it is ensured that discontinuities never directly cut through a node.

4.5.1 Diffusion equation

Figure 14(a) to (c) show some results for the different diffusion coefficients as given in Equation (2.12) for different geometrical situations (x_A and x_B), respectively. It is interesting that for all k_2/k_1-errors, second-order convergence is achieved *after a certain element number is exceeded*. Before, slightly sub-optimal results may be achieved. As expected, higher ratios of k_2/k_1 lead to larger errors. The influence of the velocity of the moving discontinuity is illustrated in Figure 14(d). It can be seen that, in general, higher velocities lead to larger errors. Only for small k_2/k_1-ratios it is sometimes found that the accuracy does not directly depend on the velocity, i.e. the error does not monotonically increase for larger velocities.

The difference of the time-stepping results to those obtained by using space-time elements, see section 3.1, is that, for space-time elements, second-order convergence is achieved starting with less elements and that the error level is lower, i.e. space-time elements are more accurate. Anyway, in view of the drastically reduced computational effort for time-stepping methods, we believe that it is an important finding that time-stepping in the XFEM is possible with second order and that it can certainly be preferable.

4.5.2 Advection-diffusion equation

Some results obtained for the advection-diffusion test case are shown in Figure 15. The findings made for the diffusion equation are basically confirmed here indicating that the presence of a linear advection term does not change the situation. A second-order convergence rate is achieved for all k_2/k_1-ratios and geometrical situations considered. It is seen in Figure 15(b) that larger velocities of the discontinuity do not necessarily lead to larger errors, although we found, that this is often the case (especially for large k_2/k_1-ratios).

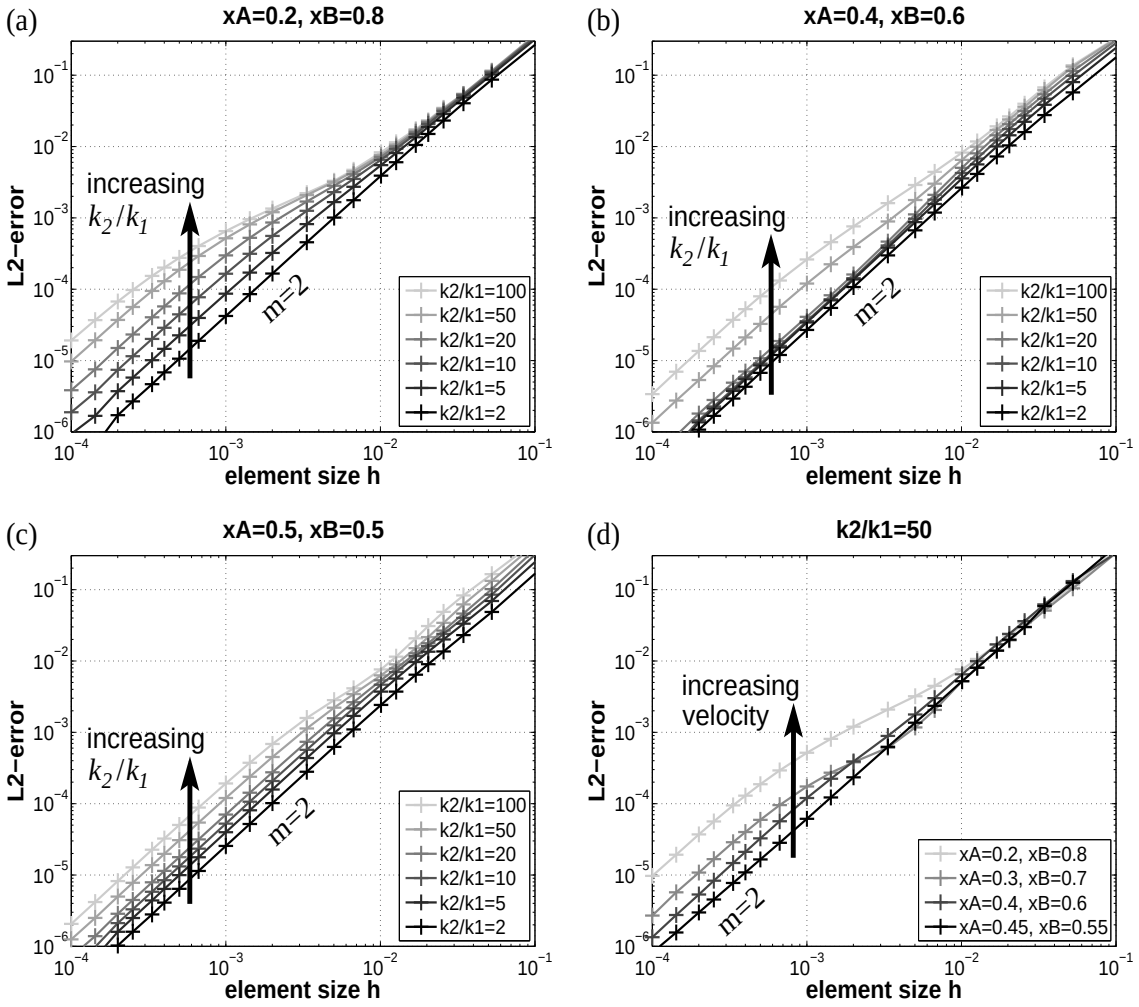

Figure 14: Convergence results for the diffusion test case. (a), (b), and (c) show the dependence of the accuracy on the k_2/k_1-ratio. (d) shows the dependence on the velocity speed.

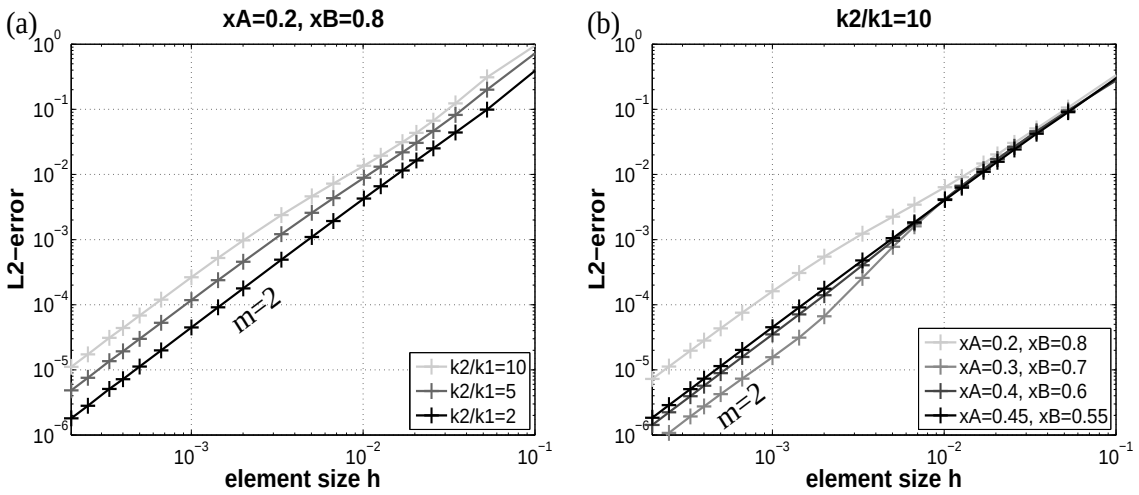

Figure 15: Convergence results for the advection-diffusion test case. (a) shows the dependence of the accuracy on the k_2/k_1-ratio. (b) shows the dependence on the velocity speed.

4.5.3 Burgers equation

Figure 16(a) to (c) show results for the trapezoidal rule with $k_1/k_2 = \{2, 5, 10\}$, respectively. In each figure, a number of different geometrical situations are considered, with discontinuity velocities ranging from $(0.8 - 0.2)/0.2 = 3$ to $(0.51 - 0.49)/0.2 = 0.1$. The element numbers in space and time are $n_x = N - 1$ and $n_y = N/5$, respectively. It may be seen that the convergence rates are inbetween 1.5 and 2.0. Thus, optimal convergence rates are not, in general, achieved for the Burgers equation. Only for small velocities and small k_1/k_2-ratios, optimal convergence rates are found. It is noteworthy, that for no velocity and k_1/k_2-ratios have we achieved a convergence rate of less than 1.5.

In Figure 17, we confirm that the problem is not in the spatial error but in the temporal error. For the case where $x_A = 0.2$, $x_B = 0.8$ and $k_1/k_2 = 10$, the spatial and temporal errors are shown. The spatial error is converged out for $n_x = N - 1$ and $n_y = (64 \cdot N)/5$, see Figure 17(a). An optimal convergence rate of 2 is achieved. Figure 17(b) shows the temporal error which is achieved for $n_x = 32 \cdot N - 1$ and $n_y = N/5$. It can be seen that only a suboptimal convergence rate of 1.5 is found.

Let us now study the (implicit) midpoint rule. The weak form is given in Equation (4.13). It is important to note that there are now three time levels involved, t_n, t_θ, and t_{n+1}. As a consequence one would need to evaluate the level-set function at all three time levels in order to evaluate the approximations u_n^h, u_θ^h, and u_{n+1}^h and the diffusion parameter k_n, k_θ,

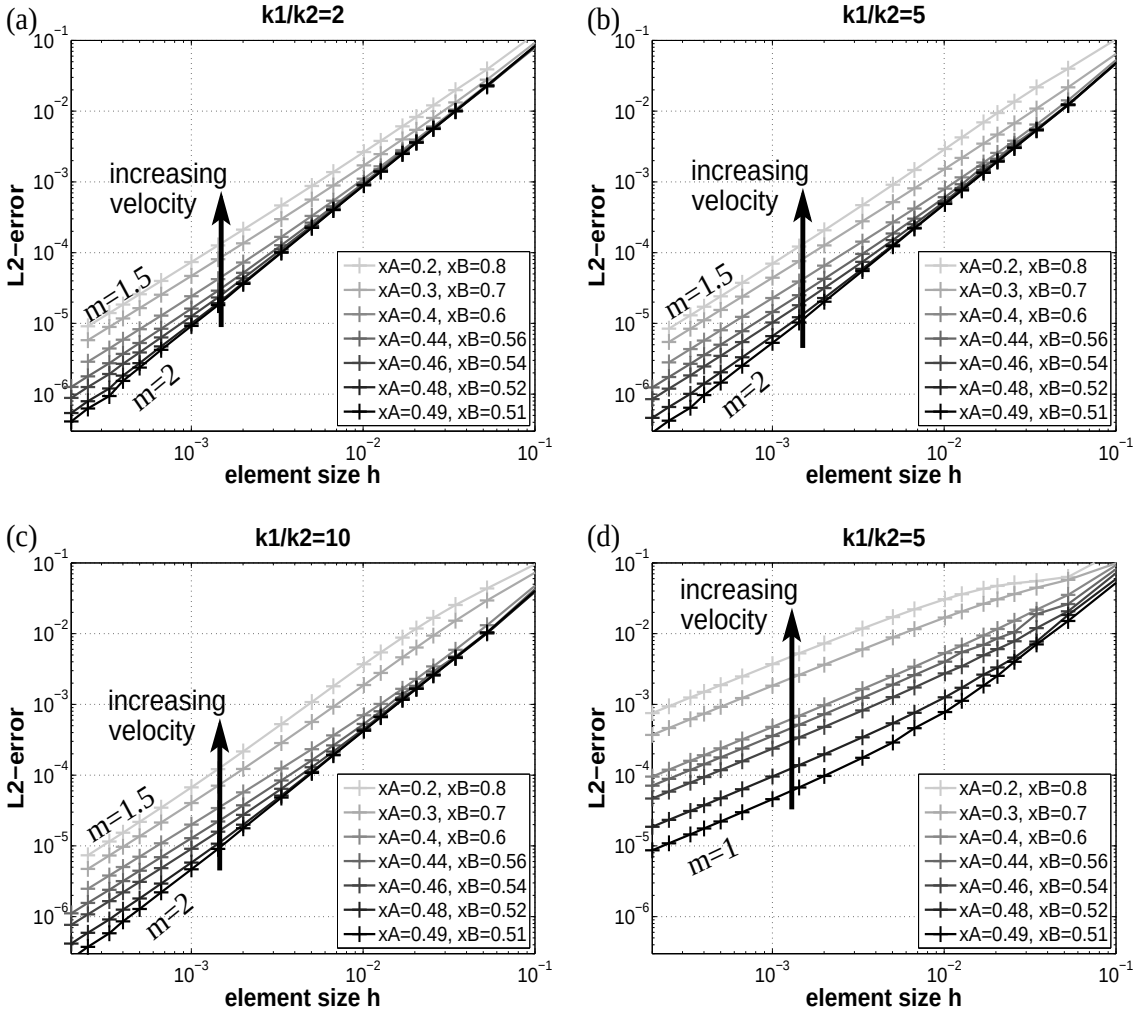

Figure 16: Convergence results for the Burgers test case. (a) to (c) show results for the trapezoidal rule, (d) for the midpoint rule.

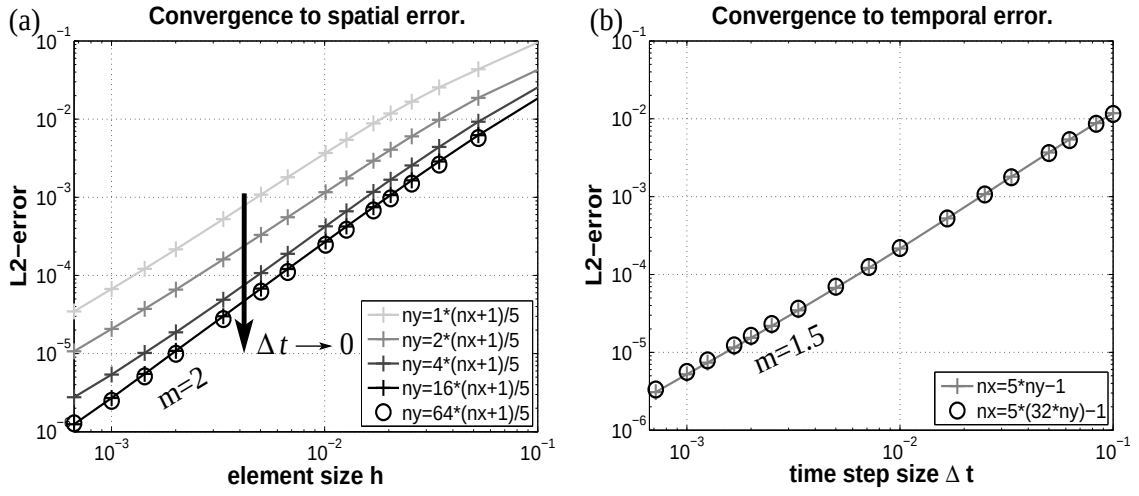

Figure 17: Convergence to (a) spatial and (b) temporal error for the trapezoidal rule.

and k_{n+1} correctly. Furthermore, the integration would need to be with respect to the three discontinuities defined by ϕ_n, ϕ_θ, and ϕ_{n+1}. The consequence would be a dramatic increase in the computational effort, especially in higher dimensions. Therefore, we interpolate u^h_θ and k_θ as follows

$$k_\theta = \theta \cdot k_{n+1} + (1-\theta) \cdot k_n, \tag{4.19}$$

$$u^h_\theta = \theta \cdot u^h_{n+1} + (1-\theta) \cdot u^h_n. \tag{4.20}$$

The decomposition of the elements for integration purposes can then be done as before for the trapezoidal rule, i.e. based on ϕ_n and ϕ_{n+1}. Figure 18 explains the difference in k_θ when using the correct and simplified definition.

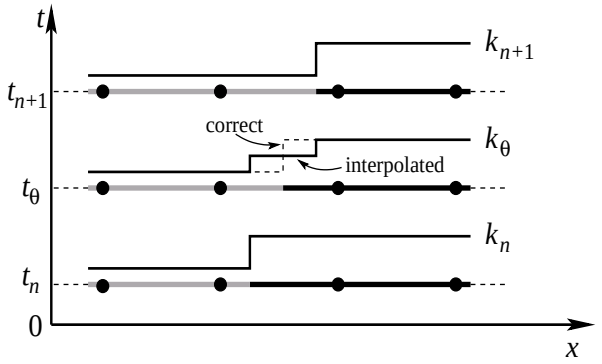

Figure 18: Difference between the interpolated and correct k_θ in the midpoint rule.

The results for the midpoint rule using the above mentioned simplifications are shown in Figure 16(d). It can be seen that only first-order convergence is achieved. We trace this error back to the interpolation for time level t_θ as described above.

5 Conclusions

In this work, the performance of time integration schemes in the XFEM for moving discontinuities is studied. Only linear elements are analyzed as higher-order elements for discontinuities are only rarely used. The discontinuous Galerkin method in time and several time-stepping schemes are examined.

For a time-stepping scheme in the XFEM, it is found that the following aspects are important:

- The temporal discretization should be done before the spatial discretization.

- The test and trial functions must be evaluated at the same time level t_{n+1}.

- Enrichment functions must be evaluated at different time levels, at least at t_{n+1} and t_n. Each evaluation is with respect to a time-dependent level-set function evaluated at the corresponding time levels.

- The quadrature must consider the position of the discontinuities at the different time levels used, at least at t_n and t_{n+1}.

Optimal or slightly sub-optimal results have been obtained by the trapezoidal rule which is, therefore, recommended for time integration in the XFEM. In contrast, the implicit midpoint rule requires a significantly higher computational effort if the additional discontinuity at $t_{n+1/2}$ is considered correctly (e.g. in the quadrature). If this is neglected, the convergence rate of the midpoint rule reduces to one for non-linear equations. The implicit Euler scheme is first order in time as expected.

For the discontinuous Galerkin method in time, it is found that enriched space-time elements enable second-order accuracy in time and the error level is generally lower than in time-stepping methods. Comparing the discontinuous Galerkin method in time with time-stepping schemes, it is noteworthy that the time-stepping schemes only need half of the unknowns (n). For many problems, the computational effort is dominated by the solver for the system of equations at least for large n. Then, with a complexity of n^2, which is typical for direct sparse system solvers, time-stepping computations require only a forth of the computing time. Furthermore, the use of the discontinuous Galerkin method in time for problems in three spatial dimensions requires four-dimensional space-time elements. In the XFEM, based on the position of the discontinuities, these 4D elements have to be subdivided for integration purposes. The complexity is obviously significantly larger compared to the situation with time-stepping methods.

Therefore, although space-time elements are also a useful choice in the XFEM, we believe that the presence of a time-stepping scheme with optimal or slightly sub-optimal convergence rates is an important achievement.

References

[1] Babuška, I.; Melenk, J.M.: The partition of unity method. *Internat. J. Numer. Methods Engrg.*, **40**, 727 – 758, 1997.

[2] Belytschko, T.; Black, T.: Elastic crack growth in finite elements with minimal remeshing. *Internat. J. Numer. Methods Engrg.*, **45**, 601 – 620, 1999.

[3] Belytschko, T.; Chen, H.; Xu, J.; Zi, G.: Dynamic crack propagation based on loss of hyperbolicity and a new discontinuous enrichment. *Internat. J. Numer. Methods Engrg.*, **58**, 1873 – 1905, 2003.

[4] Belytschko, T.; Liu, W.K.; Moran, B.: *Nonlinear Finite Elements for Continua and Structures*. John Wiley & Sons, Chichester, 2000.

[5] Belytschko, T.; Moës, N.; Usui, S.; Parimi, C.: Arbitrary discontinuities in finite elements. *Internat. J. Numer. Methods Engrg.*, **50**, 993 – 1013, 2001.

[6] Brooks, A.N.; Hughes, T.J.R.: Streamline upwind/Petrov-Galerkin formulations for convection dominated flows with particular emphasis on the incompressible Navier-Stokes equations. *Comp. Methods Appl. Mech. Engrg.*, **32**, 199 – 259, 1982.

[7] Chessa, J.; Belytschko, T.: An enriched finite element method and level sets for axisymmetric two-phase flow with surface tension. *Internat. J. Numer. Methods Engrg.*, **58**, 2041 – 2064, 2003.

[8] Chessa, J.; Belytschko, T.: An extended finite element method for two-phase fluids. *ASME J. Appl. Mech.*, **70**, 10 – 17, 2003.

[9] Chessa, J.; Belytschko, T.: Arbitrary discontinuities in space-time finite elements by level-sets and X-FEM. *Internat. J. Numer. Methods Engrg.*, **61**, 2595 – 2614, 2004.

[10] Chessa, J.; Belytschko, T.: A local space-time discontinuous finite element method. *Comp. Methods Appl. Mech. Engrg.*, **195**, 1325 – 1343, 2006.

[11] Chessa, J.; Smolinski, P.; Belytschko, T.: The extended finite element method (XFEM) for solidification problems. *Internat. J. Numer. Methods Engrg.*, **53**, 1959 – 1977, 2002.

[12] Chessa, J.; Wang, H.; Belytschko, T.: On the construction of blending elements for local partition of unity enriched finite elements. *Internat. J. Numer. Methods Engrg.*, **57**, 1015 – 1038, 2003.

[13] Dolbow, J.E.; Merle, R.: Solving thermal and phase change problems with the eXtended finite element method. *Comput. Mech.*, **28**, 339 – 350, 2002.

[14] Donea, J.; Huerta, A.: *Finite Element Methods for Flow Problems.* John Wiley & Sons, Chichester, 2003.

[15] Fries, T.P.: A corrected XFEM approximation without problems in blending elements. *Internat. J. Numer. Methods Engrg.*, DOI: 10.1002/nme.2259, 2007.

[16] Fries, T.P.: The intrinsic XFEM for two-fluid flows. *Int. J. Numer. Methods Fluids*, DOI: XX.XXXX/nmf.1901, 2008.

[17] Gerstenberger, A.; Wall, W.A.: An eXtended finite element method/Lagrange multiplier based approach for fluid-structure interaction. *Comp. Methods Appl. Mech. Engrg.*, **197**, 1699 – 1714, 2008.

[18] Groß, S.; Reusken, A.: An extended pressure finite element space for two-phase incompressible flows with surface tension. *J. Comput. Phys.*, **224**, 40 – 58, 2007.

[19] Hughes, T.J.R.; Franca, L.P.; Hulbert, G.M.: A new finite element formulation for computational fluid dynamics: VIII. The Galerkin/Least-squares method for advective-diffusive equations. *Comp. Methods Appl. Mech. Engrg.*, **73**, 173 – 189, 1989.

[20] Hughes, T.J.R.; Liu, W.K.; Zimmermann, T.K.: Lagrangian-Eulerian Finite Element Formulation for Incompressible Viscous Flows. *Comp. Methods Appl. Mech. Engrg.*, **29**, 329 – 349, 1981.

[21] Ji, H.; Chopp, D.; Dolbow, J.E.: A hybrid extended finite element/level set method for modeling phase transformations. *Internat. J. Numer. Methods Engrg.*, **54**, 1209 – 1233, 2002.

[22] Johnson, C.: *Numerical solutions of partial differential equations by the finite element method.* Cambridge University Press, Cambridge, 1987.

[23] Kölke, A.: *Modellierung und Diskretisierung bewegter Diskontinuitäten in randgekoppelten Mehrfeldaufgaben.* Dissertation, Technische Universität Braunschweig, 2005.

[24] Lambert, J.D.: *Numerical methods for ordinary differential systems: The initial value problem.* John Wiley & Sons, Chichester, 1991.

[25] Melenk, J.M.; Babuška, I.: The partition of unity finite element method: basic theory and applications. *Comp. Methods Appl. Mech. Engrg.*, **139**, 289 – 314, 1996.

[26] Menouillard, T.; Réthoré, J.; Combescure, A.; Bung, H.: Efficient explicit time stepping for the eXtended finite element method (X-FEM). *Internat. J. Numer. Methods Engrg.*, **68**, 911 – 939, 2006.

[27] Merle, R.; Dolbow, J.: Solving thermal and phase change problems with the eXtended finite element method. *Comput. Mech.*, **28**, 339 – 350, 2002.

[28] Mitchell, A.R.; Griffiths, D.F.: *The finite difference method in partial differential equations.* John Wiley & Sons, Chichester, 1980.

[29] Moës, N.; Cloirec, M.; Cartraud, P.; Remacle, J.F.: A computational approach to handle complex microstructure geometries. *Comp. Methods Appl. Mech. Engrg.*, **192**, 3163–3177, 2003.

[30] Osher, S.; Fedkiw, R.P.: *Level Set Methods and Dynamic Implicit Surfaces.* Springer Verlag, Berlin, 2003.

[31] Réthoré, J.; Gravouil, A.; Combescure, A.: A combined space-time extended finite element method. *Internat. J. Numer. Methods Engrg.*, **64**, 260 – 284, 2005.

[32] Schiesser, W.E.: *The numerical method of lines.* Academic Press, New York, NY, 1991.

[33] Sethian, J.A.: *Level Set Methods and Fast Marching Methods.* Cambridge University Press, Cambridge, 2 edition, 1999.

[34] Sukumar, N.; Chopp, D.L.; Moës, N.; Belytschko, T.: Modeling holes and inclusions by level sets in the extended finite-element method. *Comp. Methods Appl. Mech. Engrg.*, **190**, 6183 – 6200, 2001.

[35] Verwer, J.G.; Sanz-Serna, J.M.: Convergence of method of lines approximations to partial differential equations. *Computing*, **33**, 297–313, 1984.

[36] Zienkiewicz, O.C.; Taylor, R.L.: *The Finite Element Method*, Vol. 1 – 3. Butterworth-Heinemann, Oxford, 2000.

[37] Zilian, A.; Legay, A.: The enriched space-time finite element method (EST) for simultaneous solution of fluid-structure interaction. *Internat. J. Numer. Methods Engrg.*, DOI: 10.1002/nme.2258, 2007.